



Kinetics, isotherm, and optimization of the hexavalent chromium removal from aqueous solution by a magnetic nanobiosorbent

Majid Daneshvar¹ · Mohammad Raouf Hosseini¹

Received: 27 May 2018 / Accepted: 30 July 2018 / Published online: 9 August 2018
© Springer-Verlag GmbH Germany, part of Springer Nature 2018

Abstract

Sorption is the most effective approach to the treatment of acid mine drainage (AMD) and wastewaters, but the removal of the adsorbents from water has always been a challenging problem which may be resolved by using magnetic separation. In this work, a magnetic bioadsorbent was prepared using low cost and high-performance sources and applied in Cr(VI) removal from a synthetic solution. Initially, magnetite nanoparticles were synthesized from iron boring scraps by chemical co-precipitation method. Results of dynamic light scattering (DLS) and vibrating sample magnetometry (VSM) analyses showed that the synthesized nanoparticles were around 40 nm in size and had a significant magnetization. Then, the magnetite nanoparticles were attached to the dead and alkaline activated biomass of *Aspergillus niger*. Central composite design (CCD) was applied to determine the optimal condition of Cr(VI) adsorption on the produced magnetic nanobiocomposite. The maximum chromium removal (~92%) was achieved at pH 5.8, Cr concentration 23.4 mg/l, adsorbent dose 3.72 g/l, agitation rate 300 rpm, and duration 11 min. Kinetic studies showed that regardless of temperature, the process was controlled by mass transfer and intraparticle diffusion with an equilibrium constant of 0.74 mg/g min^{1/2} at 40 °C. Also, the adsorption isotherms followed the Temkin model, which indicated the physical adsorption of Cr(VI) on the produced sorbent. Therefore, the magnetic nanobiocomposite has a perfect ability to be used as the chromium adsorbent and can be collected by a low external magnetic field.

Keywords Adsorption · Fungus · Hexavalent chromium · Kinetics · Magnetite nanoparticles · Optimization

Introduction

The development of mines, industrialization, and increasing population has led to the environmental pollution by various types of heavy metal ions (Paul et al. 2006). The acid mining drainage (AMD) and the wastewaters expelled from the mineral processing mills, battery, paint, leather, and ceramics manufacturers contain a significant amount of heavy metal ions (Ahluwalia and Goyal 2007; Mondal et al. 2017;

Sivakumar 2016). Several treatment approaches like chemical precipitation, reverse osmosis, sorption, deposition, and electrolytic techniques have been applied to remove heavy metal ions from contaminated aqueous solutions (Fu and Wang 2011). Among the mentioned techniques, sorption is a low-cost, flexible, and high-performance method for the removal of heavy elements (Salam 2017), while others may encounter problems in the case of low metal concentration and dangerous wastes (Farooq et al. 2010). Recent advances in biotechnology and its application in the wastewater management have shown that the use of environment-friendly biological adsorbents is cheaper and more efficient than the conventional methods (Farooq et al. 2010; Hlihor et al. 2017; Owlad et al. 2009; Rezaei 2016; Sivakumar 2016). So far, many studies have been reported on the adsorption of the heavy metal ions by the biological adsorbents, but the separation of adsorbents from water after process completion is one of the most important challenges in all of the biological and chemical methods (Farooq et al. 2010). Recently, magnetic nanoparticles have been implemented in the adsorption of heavy metal ions due

Responsible editor: Tito Roberto Cadaval Jr

Electronic supplementary material The online version of this article (<https://doi.org/10.1007/s11356-018-2878-1>) contains supplementary material, which is available to authorized users.

✉ Mohammad Raouf Hosseini
r.hosseini@cc.iut.ac.ir

¹ Department of Mining Engineering, Isfahan University of Technology, Isfahan 8415683111, Iran

to the high surface to volume ratio and their ability to be attracted by a weak external magnetic field (Iconaru et al. 2016; Rajput et al. 2016). However, the chemical instability and the aggregation of these nanoparticles by Van der Waals forces and magnetic dipole–dipole interactions are the significant disadvantages of the magnetic nanoparticle as the heavy metal adsorbent (Ding et al. 2015). To overcome these problems, surface coatings with polymers, surfactants, biomass, and other materials are performed (Kurt et al. 2017; Sureshkumar et al. 2016). The composition of magnetic nanoparticles with microbial biomass not only protects the nanoparticles against aggregation and decomposition but also increases the adsorbent surface and efficiency. Magnetotactic bacteria which are capable of intracellular production of magnetite nanoparticles have been used as a natural magnetic biocomposite for the adsorption of heavy metal ions (Li et al. 2013; Wang et al. 2011). However, because of the low growth rate, small biomass, and tough cultivation conditions, they are not efficient in the refining of wastewaters (Lefèvre and Bazylini 2013). Fungi are the best biosorbents to be implemented in the removal of heavy elements from polluted waters due to the low cost, rapid growth, high biomass production, and convenient culturing and harvesting conditions (Sivakumar 2016). Accordingly, the application of fungi in the manufacturing of magnetic biosorbents will lead to the production of highly efficient adsorbents for eliminating the hazardous ions from wastewaters, without separation, aggregation, and decomposition problems.

As defined by the United States Environmental Protection Agency (USEPA), chromium is one of the health hazards found in the organic and inorganic pollutants (Ramos et al. 2002). Chromium ions have two stable species in nature, Cr(III) and Cr(VI). Cr(III) plays an important role in the metabolism of organisms, but it can be easily oxidized to Cr(VI) (Lv et al. 2015). Cr(VI) is highly toxic and has a high solubility and mobility (Preethi et al. 2017). The permitted concentration of the Cr(VI) compounds in drinking water is limited by the World Health Organization (WHO) to less than 0.05 mg/l (Tan et al. 2017). The Cr(VI) anionic compounds in aqueous solutions are HCrO_4^- , CrO_4^{2-} , and $\text{Cr}_2\text{O}_7^{2-}$ that their stability is dependent on the electrochemical potential and pH values of the solution (Guan et al. 2015). Cr(VI) may cause skin allergy and cancerous disease (Daraei et al. 2015). The adsorption of Cr(VI) on *Aspergillus foetidus* ($q_e = 2$ mg/g) (Prasenjiti and Sumathi 2005), *Rhizopus* sp. ($q_e = 4.33$ mg/g) (Zafar et al. 2007), *Termitomyces clypeatus* ($q_e = 24.84$ mg/g) (Fathima et al. 2015), and *Zoogloea ramigera* ($q_e = 2$ mg/g) (Nourbakhsh et al. 1994) and also, nanotubes, polymers, polymeric resins, graphene (Lv et al. 2015), and other standard adsorbents like kaolinite (6.1 mg/g), silica (1.5 mg/g), and activated nanozeolite (14.16 mg/g) have been studied (Rosales-Landeros et al. 2013).

In the present study, a magnetic nanobiocomposite is produced using the magnetite nanoparticles synthesized from iron boring scraps and the biomass of *Aspergillus niger* obtained from pistachio shell. Then, the Cr(VI) adsorption on the prepared composite was optimized, and the temperature effect, adsorption kinetics, and equilibrium isotherms were investigated in the maximized Cr(VI) removal condition.

Experimental section

Materials

Iron boring scraps (96% Fe, 4% C), hydrochloric acid 37 v/v%, and hydrogen peroxide were used for preparing an iron solution. Ammonia solution 25 wt% was used as the precipitating agent and oleic acid applied as coating surfactant. Also, ethanol was used to remove the excess coating agents. *Aspergillus niger* was obtained and purified from the pistachio shell. Poly(diallyldimethylammonium chloride) (PDADMAC) 25 wt% solution was applied as an adhesive to attach the magnetite nanoparticles on the surface of the fungus. At last, 1,5-diphenylcarbazide, potassium dichromate, methanol, phosphoric, and sulfuric acid were implemented to determine hexavalent chromium concentration by a colorimetric method. All the mentioned chemicals were of analytical grade and purchased from Merck® Company.

Synthesis of magnetite nanoparticles

Firstly, 5.86 g of the iron scraps was dissolved in 100 ml of hydrochloric acid 6.5 v/v% to prepare FeCl_2 solution (1 M). A FeCl_3 solution was obtained by adding 1 ml of hydrogen peroxide to 50 ml of the prior FeCl_2 solution. Then, the synthesis procedure was followed according to the chemical coprecipitation method (Petcharoen and Sirivat 2012). One hundred milliliters of iron solution as the initial precursor was prepared by mixing Fe^{3+} and Fe^{2+} solutions with 1:2.5 M ratio, and 0.3 ml of oleic acid was added to the iron solution at 80 °C while stirring. Then, 38.4 ml of the ammonia solution (25 wt%) was added dropwise till the solution color turned to black. The produced magnetite nanoparticles were collected by centrifuging the obtained solution at 3857×g for 10 min using a Hettich centrifuge (universal 320R, Germany) and thoroughly washed with distilled water and ethanol several times to remove the chloride ions and excess oleic acid. Finally, produced nanoparticles dried in a vacuum oven (Yaran YVO 500-64, Iran) at 50 °C for 24 h and were protected from the air for the characterization and nanobiocomposite production.

Characterization of the magnetic nanoparticles

To determine the crystalline structure of the synthesized nanoparticles, an X-ray diffractometer (XRD, Asenware AW/XDM 300, China) with Cu K α radiation source was used in the 2θ range between 10° and 100° , the scan speed of $3^\circ/\text{min}$, and the scan step of 0.05° . A dynamic light scattering device (DLS, VASCO FlexTM, Corduan, France) was employed to find the size distribution of the nanoparticles at the wavelength of 675 nm. Magnetic properties of the synthesized powders were studied by vibrating sample magnetometer (VSM, Meghnatis Daghigh Kavir Co., Iran) under 8000 G magnetic field strength at room temperature. The switching field distribution SFD and the squareness ratio SQR were calculated by the following equations (Eqs. 1 and 2) (Dodrill and Cryotronics 1999).

$$\text{SFD} = \frac{\Delta H}{H_c} \quad (1)$$

$$\text{SQR} = \frac{M_r}{M_s} \quad (2)$$

where H is the applied field, H_c is the coercivity, ΔH is the full width at the half maximum of the differentiated curve dM/dH (G), M is the magnetization of the nanoparticles, M_r is the remanence magnetization, and M_s is the saturation magnetization (emu/g) which can be obtained from the hysteresis loops.

The morphological structure of the magnetic nanoparticles was examined by transmission electron microscope (TEM, Philips, CM-120, the Netherlands). Finally, Fourier transform infrared (FT-IR) spectrometer (BRUKER, Tensor 27, USA) with a wavenumber range of 4000–400/cm was used for the functional group characterization of the magnetic nanoparticles.

Preparation of the biomass

Potato (300 g/l), glucose (20 g/l), agar (20 g/l), and distilled water were used to prepare the solid culture medium. Spores of *Aspergillus niger* were transferred to the PDA slants and cultivated in an incubator (Jaltajhiz, Iran) for 96 h at 35°C . The liquid media was prepared in a 500 ml flask containing glucose, 20 g/l; peptone, 10 g/l; KH_2PO_4 , 0.5 g/l; MgSO_4 , 0.25 g/l; NaCl, 0.2 g/l; CaCl_2 , 0.1 g/l; KCl, 0.1 g/l; and FeSO_4 , 0.005 g/l (Kapoor et al. 1999). After that, 100 ml autoclaved liquid culture medium was inoculated with the fungal spores from the PDA slants and incubated in a shaker incubator (Jaltajhiz, Iran) for 96 h at 35°C and 150 rpm. Obtained fungus biomass was filtered and washed to remove the spent liquid media. For alkaline activation, 40 g of filtered wet biomass was boiled in 500 ml of NaOH (0.5 M) solution for 15 min (Amini et al. 2009). Then, the product was washed with distilled water till the filtrate reached a neutral pH.

Preparation of the magnetic nanobiocomposite

Initially, 10 g of the activated wet biomass was mixed with 500 ml of PDADMAC 1% solution while stirring at 500 rpm for 1 h. Afterward, 0.5 g of the previously synthesized magnetite nanoparticles was added to the solution and agitated for another 1 h at 500 rpm. Finally, the magnetic nanobiocomposite was filtered and washed to remove the uncoated nanoparticles from the surface of the biomass. Moreover, scanning electron microscope (SEM) picture and energy-dispersive X-ray spectroscopy (EDS) analysis of the composite were obtained using a field emission scanning electron microscope (FE-SEM, Mira 3-XMU, Czech) and was used to confirm the attachment of the magnetite nanoparticles on the surface of the biomass.

Optimization of Cr(VI) adsorption

Chromium adsorption experiments were performed at 30°C using a synthetic Cr(VI) solution prepared by dissolving potassium dichromate in distilled water. Effective parameters were optimized by using a central composite design (CCD). The values of the parameters including pH, agitation rate, initial Cr(VI) concentration, adsorbent dosage, and adsorption time were set at five levels which are summarized in Table 1.

The response surface methodology matrix contains 50 runs (Table S1) representing the relationship between the design variables and the responses (Cr residual concentration, adsorption capacity, and Cr removal percent) by a regression equation which is also employed to determine the optimum value of each variable. After obtaining the optimal values, the adsorption tests were carried out at 30, 40, 50, and 60°C to find out the effect of temperature on the adsorption process.

Determination of the chromium concentration

Hexavalent chromium solution was colored by 1,5-diphenylcarbazid, and the color intensity was measured by a spectrophotometer (Unico 2100, USA) at 540 nm (Mondal et al. 2017). Adsorbent capacity and Cr(VI) removal percent were calculated by Eqs. 3 and 4, respectively.

$$q = \frac{(C_i - C_f)}{m} \quad (3)$$

$$r = \frac{(C_i - C_f)}{C_i} \times 100 \quad (4)$$

where q is the adsorbent capacity (mg/g), r is the removal percent, C_i and C_e are the Cr(VI) initial and final concentrations (mg/l), respectively, and m is the adsorbent dosage (g/l).

Kinetics and isotherm studies

Kinetics of Cr(VI) adsorption by the magnetic nanobiocomposite was investigated at four different

Table 1 The experimental variables and their levels in the CCD design

Effective parameters	Parameter levels				
	2.37	1	0	−1	−2.37
pH	8	6	4.5	3	1
Agitation rate (rpm)	500	384	300	216	100
Cr(VI) concentration (mg/l)	60	44	32.5	21	5
Adsorbent dosage* (g/l)	5	3.84	3	2.16	1
Time (min)	60	45.5	35	24.5	10

*Dry weight

temperatures using the optimum condition obtained from the CCD design. Sampling was done at regular 1-min intervals. The empirical pseudo-first-order and pseudo-second-order models along with phenomenological Weber and Morris model (Weber and Morris 1962) were fitted to the kinetic data, and the rate of Cr(VI) adsorption was calculated. To determine the adsorption isotherm model of Cr(VI) removal by the composite, the Langmuir, Freundlich, Temkin, and Dubinin–Radushkevich (D–R) adsorption isotherm models were fitted to the adsorption results obtained from seven levels of initial Cr(VI) concentrations (5, 10, 20, 30, 40, 60, and 80 mg/l). Also, adsorption mechanism and equilibrium capacity were calculated from each isotherm model. The kinetic and isotherm tests were performed in duplicate, and all the mentioned model equations are given in Tables S2 and S3, respectively.

Comparative tests

To determine and compare the adsorption ability of each synthesized adsorbents, a series of comparative adsorption tests were conducted in duplicate at 40 °C using the optimum condition obtained by the CCD design. The applied adsorbents were raw, alkaline activated, polymer-treated activated biomass, magnetite-raw biomass composite, magnetic nanobiocomposite, and the bare magnetite nanoparticles. Each biological adsorbent (3.72 g/l) was used to treat the synthetic solutions with 23.37 g/l chromium concentration. Also, the concentration of the magnetite nanoparticles as adsorbent was 6 mg/l which was equal to the magnetite content of the produced nanobiocomposites.

Results and discussion

Characterization of the synthesized magnetic nanoparticles

Figure 1a–c shows the prepared composite and its reaction to an external magnetic field. The SEM image of the magnetic nanobiosorbent proves the successful stabilization of the

magnetic nanoparticles on *A. niger* biomass (Fig. 1d). Also, the EDS analysis on the composite is presented in Fig. 1e. Oxygen and carbon peaks confirm the presence of fungal biomass, and the detected iron element is attributed to the attached magnetite nanoparticles. An XRD analysis was performed to investigate the crystal structure of the synthesized magnetic nanoparticles. Figure 2a shows the diffraction peaks at 30.14°, 35.5°, 43.1°, 57.2°, 62.6°, and 89.7° which are related to the (112), (103), (004), (321), (224), and (127) lattice planes, respectively. They indicate that the nanoparticles are magnetite (Fe₃O₄) with an orthorhombic crystalline structure (JCPDS 01-075-1609). The crystalline size of the synthesized magnetite nanoparticles was found to be 27.48 nm by using Scherer’s equation (Eq. 5).

$$d_p = \frac{k\lambda}{\beta \cos\theta} \tag{5}$$

where d_p is the crystalline size (nm), k is the shape factor (0.89), λ is the X-ray wavelength (0.154 nm), β is the full-width at the half-maximum (FWHM) of the strongest peak (in radians), and θ is the Bragg’s angle.

The particle size distribution diagram derived from DLS analysis is presented in Fig. 2b and indicates that the mean size of the magnetite nanoparticles is 42 nm with a narrow dimension range. Therefore, comparing the crystalline size which was calculated from XRD results and the particle size obtained from DLS data, each particle is formed from 1.52 crystals in average.

The orthorhombic crystal structure of the particles is observable in the TEM image which is illustrated in Fig. 2c. The particle dimensions seen in the TEM image are similar to the result of the DLS analysis.

Figure 2d demonstrates the hysteresis loop of the magnetite nanoparticles. The remanence magnetization (M_r), saturation magnetization (M_s), coercivity (H_c), switching field distribution (SFD), and the squareness ratio (SQR) parameters are 5.07, 60, 62.62, 18.51, and 0.084 respectively, which were obtained from VSM analysis data. Also, considering the outputs of the particle size measurements (TEM pictures and VSM analyses), the synthesized magnetite nanoparticles have a single domain structure (Li et al. 2017).

Finally, the FT-IR spectra of the synthesized magnetic nanoparticles are shown in Fig. 2e. The vibration of the Fe–O bond in the magnetite structure appeared at 617/cm (Fatahian et al. 2012). The peak of O–H stretch bond arose at 3420/cm. The peak at 2924/cm is assigned to the asymmetric –CH₂ stretch (Zhang et al. 2006). Replacement of the surface iron atoms of the magnetic nanoparticles with hydrogen atoms of the oleic acid hydroxyl groups (Fig. 2f) has caused a red shift in C=O stretch bond from 1710 to 1047/cm. Also, bonding of iron atoms at the surface of the magnetic nanoparticles with the oxygen atoms of the oleic acid carbonyl groups made a red shift from 1710 to 1408/cm (Zhang et al. 2006).

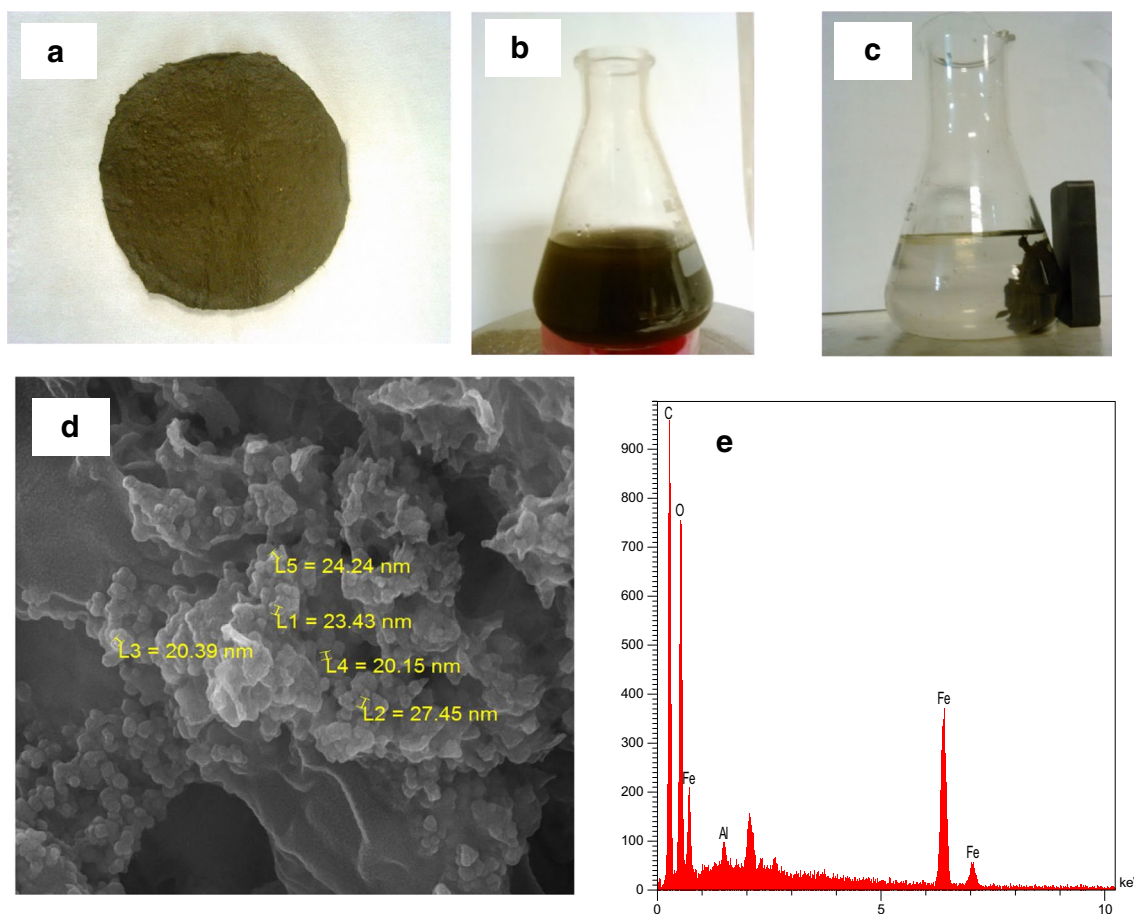


Fig. 1 Prepared magnetic nanobiocomposite **a** after washing and filtration, **b** after dispersion in water, and **c** in the presence of an external magnetic field. **d** SEM micrograph and **e** EDS analysis of the synthesized nanobiocomposite

So, the oleic acid molecules have coated the surface of the magnetic nanoparticles by bonding their oxygen to the iron atoms.

Analysis of the experimental design

The CCD design was analyzed considering the remaining Cr concentration, Cr adsorption capacity, and Cr removal percent as the response variables. Initially, polynomial equations were selected for modeling the three obtained responses based on the input variables. Then, analysis of variance was performed on the obtained data and the insignificant parameters were omitted from the model. Finally, the derived polynomial model and its associated statistics are presented in Table 2.

Remained chromium concentration as the response variable

According to the result of the ANOVA analysis presented in Table S4, three main variables including the initial concentration of chromium (C), adsorbent dosage (D), and pH (A) significantly influence the response variable, respectively, with the confidence level of more than 95%. Also, the agitation rate

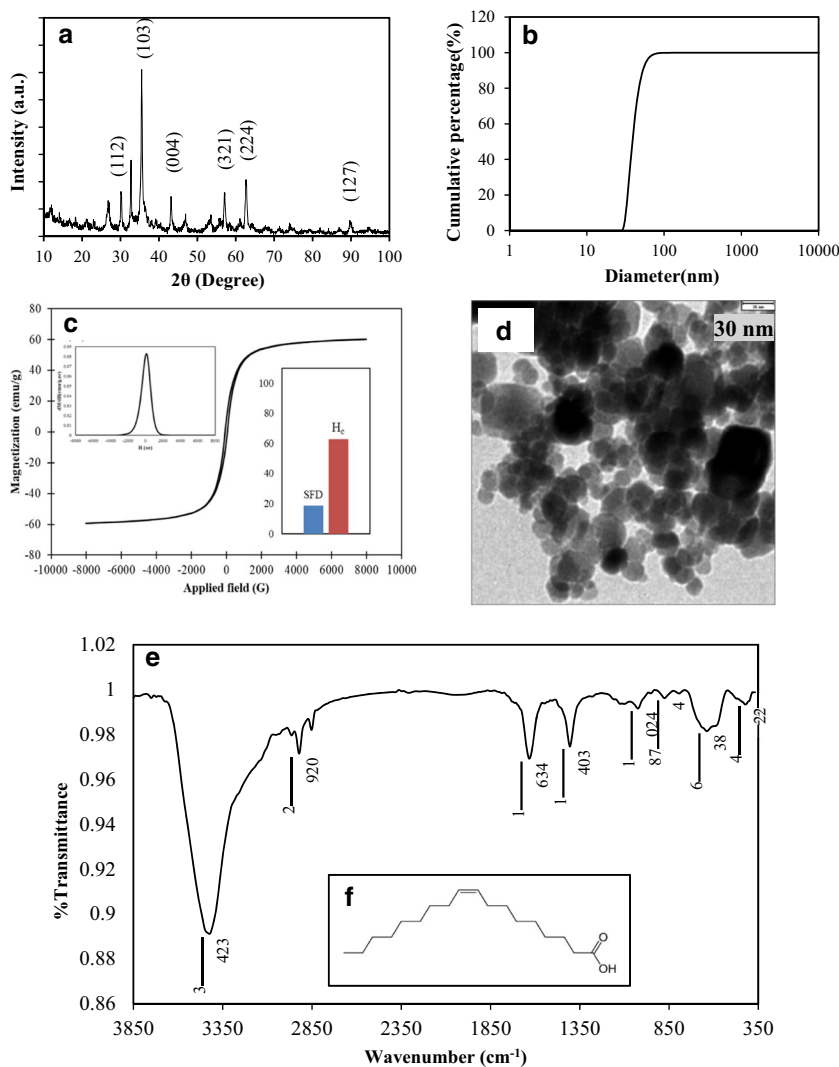
(E) can be considered effective with more than 90% confidence level. However, the adsorption time is not significant. Considering the kinetic study of the process which will be discussed later in “[Determination of the Cr\(VI\) adsorption isotherm](#),” the adsorption speed is very high and completes after about 10 min, so the Cr concentration did not vary very much in the investigated time.

Despite the adsorption time is not considered an effective variable, its interactions with pH (AB) and adsorbent dosage (BD) are very important. Other significant two-way interactions are between adsorbent dosage and pH (AD), Cr concentration (CD), and agitation rate (DE). The CE interaction (Cr concentration-agitation rate) is also effective. Further significant interactions are listed in Table S4.

The 3D interaction plots of the effective parameters are illustrated in Fig. 3. Each graph shows the effects of two parameters on the remained Cr(VI) in solution while the other parameters are at their central level (Table 1).

As the Fig. 3a indicates, the influence of the pH value is a little complicated. In shorter adsorption durations, increasing the pH of the environment is in favor of the Cr adsorption and reduces the residual chromium in the solution. At higher pH

Fig. 2 Characterization studies on the synthesized magnetite nanoparticles. **a** XRD pattern. **b** Particle size distribution diagram. **c** Magnetization hysteresis loop. **d** TEM image. **e** FT-IR spectra. **f** The oleic acid structure



values, CrO_4^{2-} is the dominant chromium ion which is electrostatically adsorbed on the positive amine groups of the fungal biomass and ferric/ferrous sites of the magnetite nanoparticles. By elongating the adsorption time, the residual Cr concentration increases which means that increasing the process duration cancels out the positive influence of the pH raise. Since the final pH values of the synthetic solutions after long-time adsorption processes were in the range of 5.8 to

6.3, it is expected that the buffering property of the sorbent to be responsible for the observed offset. Moreover, the competitive adsorption of OH^- and CrO_4^{2-} ions in a basic environment may cause a decrement in adsorption efficiency. However, at lower pH values, the functional groups (amine groups) are protonated which leads to the electrostatic adsorption of the chromium ions in the form of HCrO_4^- without any interference.

Table 2 Statistical parameters of the proposed models

Std. dev.	Mean	C.V. %	PRESS	R^2	Adj. R^2	Pred. R^2	Adeq. precision
Response: residual Cr concentration							
1.14	15.23	7.52	113.35	0.98	0.97	0.94	43.40
Response: adsorption capacity							
0.39	6.06	6.40	12.64	0.98	0.97	0.96	45.36
Response: Cr removal percent							
3.74	53.17	7.04	1306.43	0.91	0.85	0.72	23.24

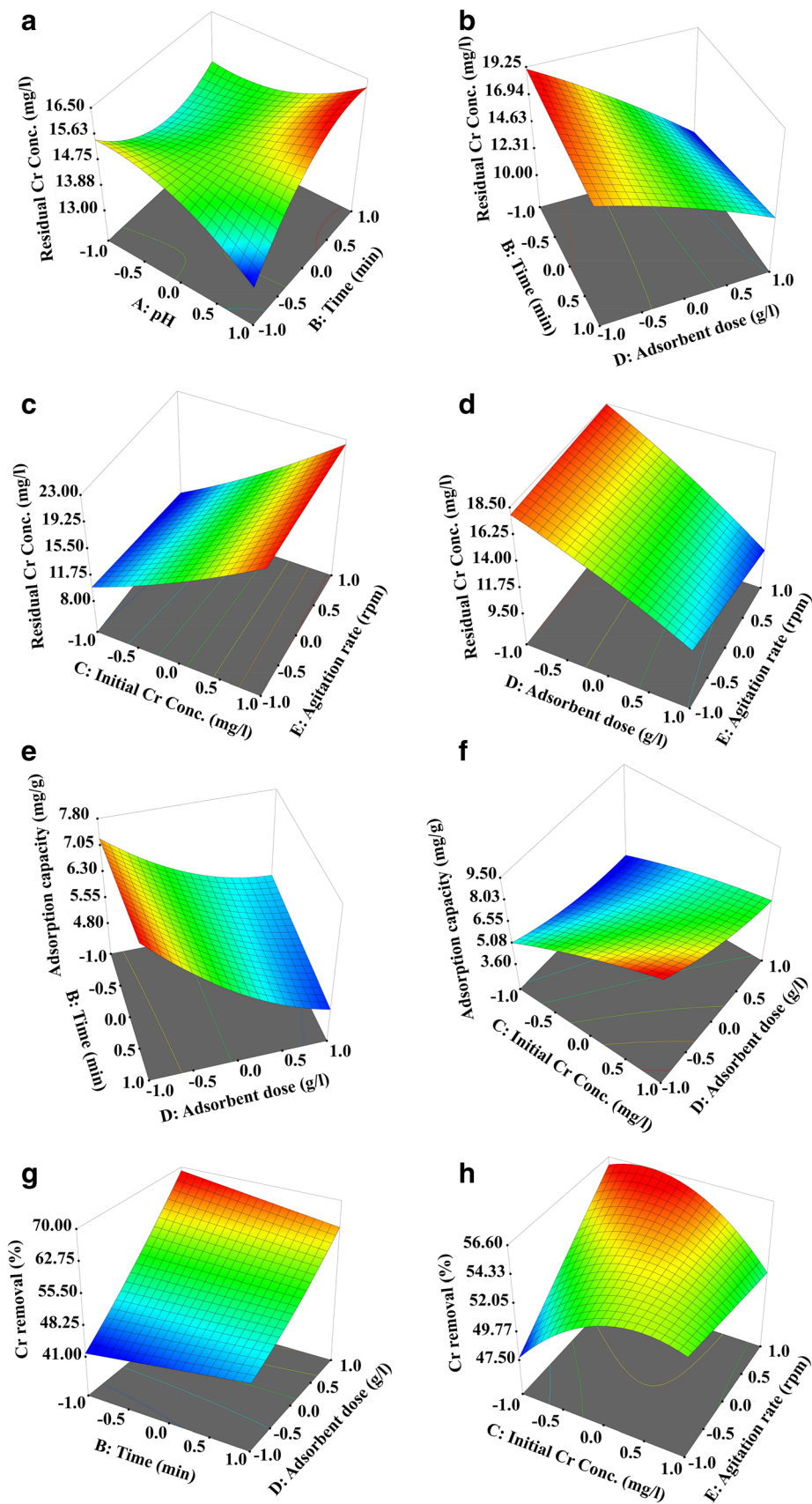


Fig. 3 3D interaction plots of the effective parameters on the Cr(VI) adsorption process

Figure 3b demonstrates the interaction plot between the adsorption time and adsorbent dosage. Overall, adsorbent dosage has a reverse relationship with the residual hexavalent chromium concentration. Reduction in the concentration of the remained Cr ions in the solution at the high adsorbent dosage is related to the increase of the adsorption active sites. However, as mentioned before, the adsorption time seems to have a trivial effect on the chromium adsorption as extending the process duration did not change the final concentration of Cr in the synthetic solution.

According to Fig. 3c, the variation of the agitation rate has no significant effect on the remaining concentration of chromium either at the bottom or at the top level of the initial Cr concentration. Variation in the response is more negligible especially at high initial Cr concentration, due to the saturation of the adsorbent active sites. Moreover, rising the initial concentration increases the remained chromium ions in the solution after the sorption process.

The effect of adsorbent dosage and agitation rate on the Cr(VI) final concentration is shown in Fig. 3d. Increasing the agitation rate reduces the thickness of the boundary layer and improves the adsorption rate in a diffusion controlled process which finally causes a reduction in the remained Cr(VI) concentration. For this reason, when the agitation rate is at its top level, the same amount of adsorbent removes more chromium ions from the solution. However, at the low level of adsorbent, changing the agitation rate does not vary the residual Cr concentration.

Finally, the remaining chromium concentration in the solution can be predicted using the coded variables and the following polynomial equation (Eq. 6).

Residual Cr concentration (mg/l)

$$\begin{aligned}
 &= 14.96 + 0.74A + 6.44C - 3.59D - 0.32E + 0.89A.B \\
 &+ 0.36A.D + 0.89B.D - 0.42C.D \\
 &+ 0.64C.E - 0.58D.E \\
 &+ 0.66C^2 - 0.36D^2 - 0.61A.C.D + 0.42B.C.D \\
 &+ 0.58A^2.B - 0.84A^2.C + 2.25A^2.D - 0.94A.B^2 \quad (6)
 \end{aligned}$$

Adsorption capacity is defined as the ratio of the adsorbed chromium mass (mg) to the sorbent mass (g). Since the adsorption capacity and the residual chromium concentration are inter-connected, the effects of the parameters on both responses are similar (Table S5).

Figure 3e indicates that the adsorbent dosage has an adverse effect on the adsorption capacity. At the low adsorbent dosage, the Cr ions adsorb on the surface of the magnetic nanobiocomposite and also diffuse into the bulk of the biomass, while at the high adsorbent dosage, the diffusion rate decreases due to the dominance of the surface adsorption. This could be the reason for the observed decline in the adsorbent

capacity at the high levels of adsorbent dosage. The adsorption mechanism will be described in detail in “[Determination of the Cr\(VI\) adsorption isotherm.](#)”

Moreover, Fig. 3f shows the interaction plot between the initial Cr(VI) concentration and the sorbent dosage. Increasing the initial concentration boosts the adsorption capacity, because the chromium adsorption improves under the influence of the concentration gradient between the bulk of the solution and sorbent surface. This gradient causes intraparticle diffusion and saturation of the active sites.

Equation 7 shows the mathematical model derived by the CCD experimental design. The adsorption capacity of the nanobiosorbent can be predicted by substituting the parameters with the related codes.

$$\begin{aligned}
 \text{Adsorption capacity (mg/g)} &= +5.86 - 0.25A + 1.69C - 1.23D \quad (7) \\
 &- 0.33A.B - 0.15A.D + 0.12A.E + 0.16B.C - 0.26B.D - 0.44C.D \\
 &- 0.25C.E + 0.19D.E - 0.22C^2 + 0.44D^2 + 0.22A.C.D \\
 &- 0.19B.C.D + 0.13C.D.E + 0.40A^2.C + 0.36A.B^2
 \end{aligned}$$

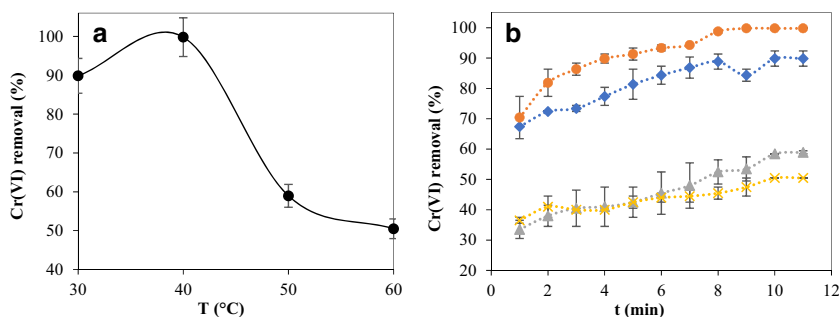
Chromium removal as the response variable

Chromium removal is one of the basic responses for determination of the adsorption efficiency. The adsorbent dosage (D), agitation rate (E), and pH (A) have significant effects on the response variable, respectively, with confidence levels of more than 95%. Regarding the definition of Cr removal percent which is the ratio of the mass of the adsorbed ions to the total mass of the ions, the Cr initial concentration is not considered a significant factor. Also, as stated before, the exclusion of time from the model parameters is an indication of the high speed of the adsorption reaction. Moreover, the influential interactions in the order of importance are the time–pH (AB), time–adsorbent dosage (BD), Cr initial concentration–agitation rate (CE), and the interaction between adsorbent dosage and pH (AD). Other significant interactions are listed in Table S6.

According to the Fig. 3g, although the adsorption time has a negligible effect on the chromium removal, its influence at low and high levels of adsorbent dosage is inverse. If a small amount of sorbent is used, longer time is needed for chromium removal, but it seems that short adsorption duration is enough for a large dosage of sorbent.

Figure 3h plots the effects of Cr(VI) initial concentration and agitation rate on the chromium removal. Raising the agitation rate increases the external velocity of the fluid which brings about a reduction in the resistance of the external surface film on the sorbent (Allen et al. 1989) which subsequently causes the highest Cr(VI) adsorption at low initial concentration. Also, raising the initial concentration to the higher levels increases the sorption motive force and enhances the Cr adsorption process. However, at the high agitation rates, the adsorbent active sites become saturated and the amount of

Fig. 4 The effect of adsorption temperature on the **a** maximum removal of Cr(VI) and **b** Cr(VI) removal during the adsorption time (filled diamond, 30 °C; filled circle, 40 °C; filled triangle, 50 °C; multiplication sign, 60 °C)



chromium removal declines by raising the initial concentration. Indeed, at concentrated chromium solution, agitation speed does not perceptively affect the Cr removal percent.

Generally, the Cr removal percentage can be calculated based on the coded parameters using the mathematical equation presented in Eq. 8.

$$\begin{aligned} \text{Cr removal percent (\%)} = & +54.34 - 2.27A + 11.05D + 1.63E \quad (8) \\ & - 3.01A.B - 2.03A.D + 1.33A.E + 1.88B.C - 2.62B.D + 1.26B.E \\ & - 2.52C.E + 1.83D.E - 2.50C^2 + 1.16D^2 + 2.60A.C.D \\ & + 1.19B.D.E - 2.45A^2.B - 6.88A^2.D + 3.01A.B^2 \end{aligned}$$

Optimization of the effective parameters

Based on the obtained models, an optimized condition was selected to minimize the residual Cr concentration and

therefore to maximize the Cr removal from the solution. The proposed criteria were pH 5.8, agitation rate 300 rpm, Cr initial concentration 23.4 mg/l, adsorbent dosage 3.72 g/l, and adsorption time 11 min. Conducting the adsorption experiment using the mentioned values at 30 °C, chromium residual concentration reached 1.88 mg/l, 91.95% of the Cr content was eliminated, and the adsorption capacity was 5.81 mg/g.

On the other hand, the optimum condition to achieve the maximum absorption capacity is different and is as follows: pH 1, agitation rate 216 rpm, Cr initial concentration 37.04 mg/l, adsorbent dosage 2.16 g/l, and adsorption time 25.58 min. In this situation, the adsorption capacity reached to 14.38 mg/g, 83.85% of the Cr content was removed, and the final chromium concentration reduced to 5.98 mg/l. It is noteworthy that this condition is too close to acid mine drainages (AMD) since

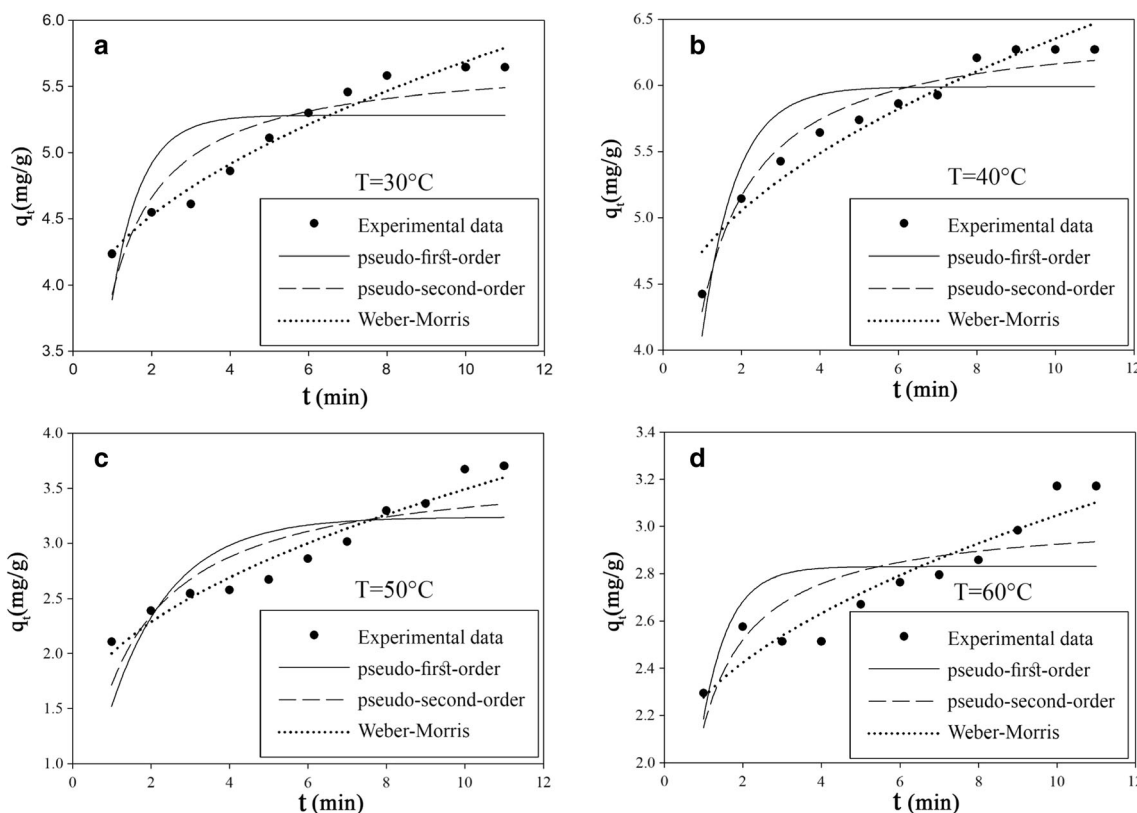


Fig. 5 Fitting the kinetic models on the experimental data at different temperatures: **a** 30 °C, **b** 40 °C, **c** 50 °C, **d** 60 °C (q_t is the adsorption capacity in the specified time)

Table 3 Parameters of the kinetic models applied to Cr(VI) adsorption data

Kinetic model	Kinetic parameters	Temperatures (°C)				R^2			
		30	40	50	60	30	40	50	60
Pseudo-first order	k_1 (/min)*	1.33	1.16	0.63	1.47	0.50	0.77	0.53	0.37
	q_e (mg/g)*	5.28	5.98	3.23	2.83				
Pseudo-second order	k_2 (g/mg/min)	0.38	0.30	0.23	0.78	0.82	0.95	0.74	0.65
	q_e (mg/g)	5.71	6.47	3.18	3.04				
Weber–Morris	k_1 (mg/g min ^{1/2})	0.66	0.74	0.68	0.35	0.96	0.93	0.94	0.90
	q_e (mg/g)	3.57	4.00	1.31	1.92				

* k and q_e are the predicted adsorption rate and final adsorbent capacity, respectively

the solution is very acidic. Therefore, it is possible to predict the results of absorption process in such circumstances.

In the next sections, the adsorption temperature is optimized using the maximum chromium removal condition, and the process models and mechanisms are studied based on the adsorption kinetics and isotherms.

Kinetic study of the adsorption process

Firstly, the effect of process temperature on the sorption efficiency was investigated by setting the temperature at 30, 40, 50, and 60 °C. Results (Fig. 4) clearly shows that increasing the temperature from 30 to 40 °C improved the sorption efficiency by removing 99.81% of Cr(VI) and remaining only 0.04 mg/l of the dissolved chromium in the prepared solution. Further augmentation of the sorption temperature to 50 and 60 °C reduced the chromium removal to 58.94 and 50.47 mg/l with the final Cr concentrations of 9.60 and 11.57 mg/l, respectively. The observed phenomenon indicates that the Cr(VI) sorption on the *A. niger* biomass is probably a physical process.

Empirical and phenomenological models including pseudo-first-order, pseudo-second-order, and Weber and Morris models were applied to the kinetic data obtained at the four temperatures (Fig. 5a–d), and the parameters of the kinetic models along with the associated correlation coefficients are presented in Table 3.

Adsorption processes typically involve three steps: (1) diffusion from bulk phase to the boundary layer (mass transfer), (2) diffusion through the boundary layer to the surface of the sorbent (intraparticle diffusion), and (3) binding on the surface functional groups. If the intraparticle diffusion dominates in adsorption process, the plot of q_t versus $t^{0.5}$ (Weber and Morris model) is a straight line and the intercept passes through the origin.

Considering the experiment conducted at 40 °C, the correlation coefficient (R^2) of the pseudo-second order model (0.95) is comparable with the Weber and Morris model (0.93) which implies that the sorption process, at this temperature, may also be simulated by an empirical model.

Nevertheless, overall results prove that the chromium sorption kinetic data at any temperature are very well described by the Weber and Morris model. The interception of the vertical axis at positive values indicates that Cr(VI) sorption using the prepared magnetic nanobiocomposite is probably controlled by both mass transfer and intraparticle diffusion.

Regarding the three phases of adsorption, it is possible to plot the linear diagram of the Weber and Morris model for each step and determine the rate of transfer, diffusion, and adhesion of the chromium ions. The shape of the Figure 6 confirms that mass transfer is also effective in the absorption process and the intraparticle diffusion alone is not the rate limiting step. Also, Fig. 6 denotes that the kinetic constant and equilibrium concentration of the adsorption steps: (1) diffusion from bulk phase to the boundary layer of the fungal biomass or magnetite nanoparticles with the rate (k_1) of 1.21 mg/g min^{1/2} and $q_e = 3.29$ mg/g, (2) diffusion through the boundary layer to the surface of the nanobiosorbent with the rate (k_1) of 0.62 mg/g min^{1/2} and $q_e = 4.43$ mg/g, and (3) binding on the surface functional groups of the sorbent ($k_1 = 0.11$ mg/g min^{1/2}, $q_e = 5.89$).

Arrhenius equation was implemented to determine the adsorption activation energy using the kinetic data. Firstly, the kinetic constants (k) at each temperature were derived from the intraparticle diffusion models (Table 3), and then the adsorption activation energy was calculated from Eqs. 9 and 10 by depicting $\ln(k)$ versus $1/T$ (Fig. 7).

$$k = A \cdot \exp\left(-\frac{E_a}{RT}\right) \tag{9}$$

$$\ln k = \ln A - \frac{E_a}{R} \cdot \frac{1}{T} \tag{10}$$

where A is the Arrhenius constant, R is the gas constant (8.314 j/mol K), E_a is the adsorption activation energy (j/mol), and T is temperature (K).

Accordingly, the obtained activation energy is 0.255 kJ/mol, which is very small and is another indication of the physical sorption that causes the rapid adsorption of chromium ions by the magnetic nanobiocomposite.

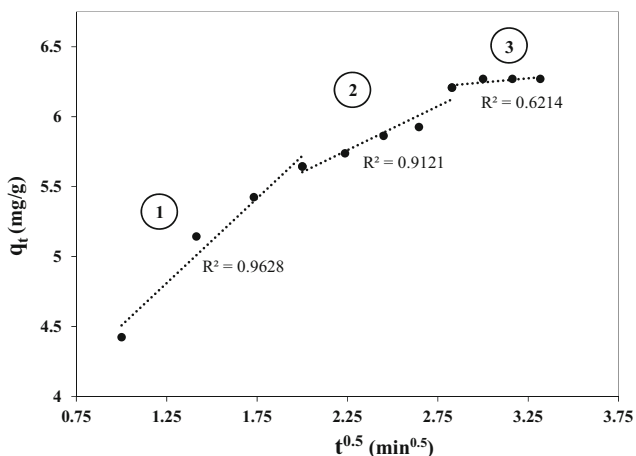


Fig. 6 Weber–Morris intraparticle diffusion plot for Cr(VI) adsorption at 40 °C

Determination of the Cr(VI) adsorption isotherm

To determine an appropriate adsorption isotherm model, final adsorbent capacity (q_e) versus final Cr(VI) concentration (C_e) diagram should be obtained.

Therefore, Langmuir, Freundlich, Temkin, and Dubinin–Radushkevich isotherm models were fitted on the experimental data (Fig. 8). The results of the model matching are summarized in Table 4. Regarding the information presented in the table, Temkin can be the best model for describing the isotherm of Cr(VI) adsorption on the produced magnetic nanobiocomposite which again confirms the physical adsorption.

Effect of adsorbent preparation steps on the Cr(VI) removal efficiency

In order to determine the importance of each stage in the magnetic nanobiosorbent manufacturing procedure, the Cr(VI) adsorption ability of the product obtained from each preparation step was examined. So, the adsorption tests were carried out at 40 °C and in the optimal condition obtained

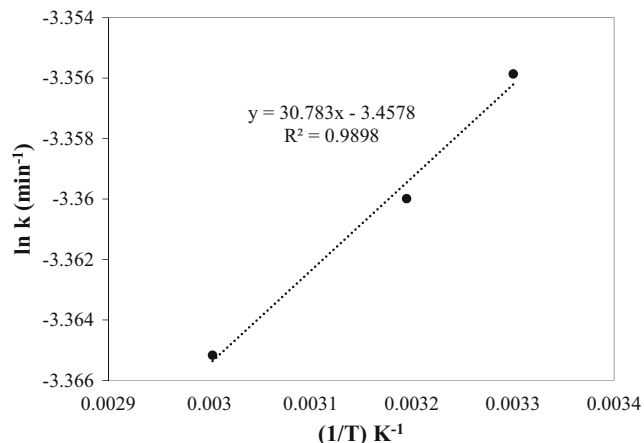


Fig. 7 Plot of $\ln k$ vs. $1/T$ fitted on the linear equation

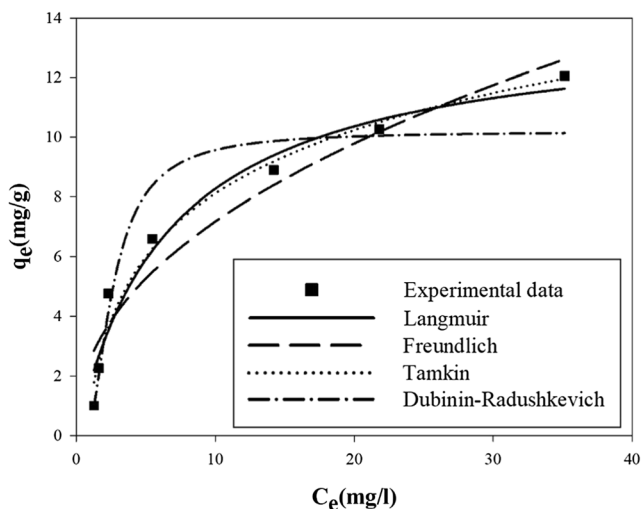


Fig. 8 Plot of adsorption isotherm data fitted with conventional isotherm models

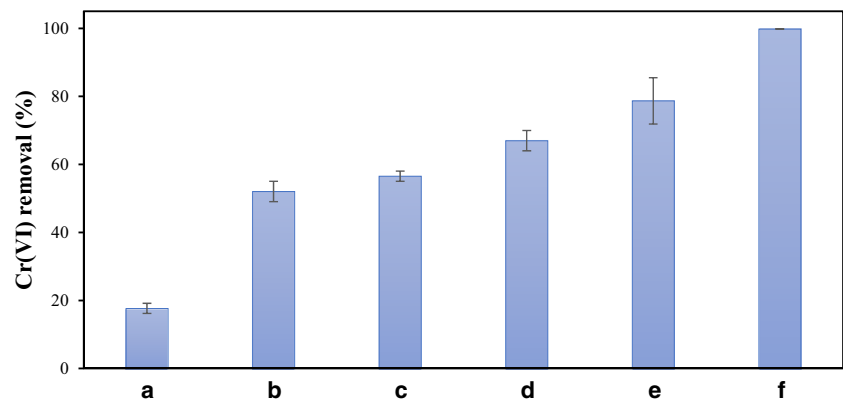
from the CCD design using six different types of adsorbent to know the effects of alkaline activation, polymer addition, and nanoparticle inclusion on the adsorption efficiency. Outcomes are illustrated in Fig. 9. Results show that the alkaline activation of *Aspergillus niger* mycelia by 0.5 M NaOH solution has a significant impact on increasing the surface functional groups and subsequently enhancing the adsorption efficiency up to 34.44%. However, polymer addition reduces the sorption ability, probably because of decreasing the electrostatic potential of the biomass surface and occupying the active sites. Also, stabilization of magnetite nanoparticle on the surface of raw and activated biomass upgraded the Cr removal by 38.34 and 32.82%, respectively, due to the high surface to volume ratio of these nanoparticles. Application of bare magnetite nanoparticles leads to 78.68% Cr(VI) removal. Therefore, using the activated biomass and magnetite nanoparticles together synergistically improves the adsorption efficiency of the produced nanobiocomposite as Cr(VI) sorbent.

Table 4 Parameters of the isotherm models fitted to Cr(VI) adsorption data

Isotherm model	Isotherm parameters	R^2
Langmuir	q_{max} (mg/g)	14.64
	K_L (L/mg)	0.14
Freundlich	K_F (mg/g)	2.55
	n	2.22
Temkin	B_T (J/mol)	3.07
	a_T (l/mg)	1.4
Dubinin–Radushkevich	q_m (mg/g)	10.19
	b_{DR} (mol ² kJ ⁻²)	1.02×10^{-6}
	E (kJ/mol)	0.27

q_{max} , q_m maximum adsorption capacity, B_T Temkin constant which is related to the heat of sorption, b_{DR} Dubinin–Radushkevich constant, a_T Temkin isotherm constant, K_F Freundlich isotherm constant, k_L Langmuir isotherm constant, $1/n$ adsorption intensity

Fig. 9 Results of the comparison study on the chromium removal abilities of the **a** raw biomass, **b** raw nanobiocomposite, **c** polymer treated activated biomass, **d** activated biomass, **e** magnetite nanoparticles, and **f** magnetic nanobiocomposite



Conclusion

A magnetic nanobiocomposite was prepared using magnetite nanoparticles synthesized from iron boring scraps and chemically modified biomass of *A. niger*. Then, the capability of the invented sorbent for treating wastewaters and acid mine drainages (AMD) was examined by removing Cr(VI) ions from a synthetic solution in acidic and alkaline environments. Optimization studies on the chromium removal indicate that increasing pH, adsorbent dosage, and agitation rate enhance the adsorption process, and in the best condition can eliminate Cr(VI) from slightly or extremely acidic solutions by 92 and 84%, respectively. Generally, results of the kinetics and isotherm analyses show that the adsorption of hexavalent chromium by the invented adsorbent is physical and controlled by both of the mass transfer and intraparticle diffusion mechanisms. The high sorption rate is due to the low activation energy of adsorption and high density of the active sites on the adsorbent surface which removes about 70% of Cr(VI) within 1 min. Therefore, thanks to high and multilayer adsorption capacity, the prepared composite is capable of treating wastewaters and acid mine drainages (AMD).

References

- Ahluwalia SS, Goyal D (2007) Microbial and plant derived biomass for removal of heavy metals from wastewater. *Bioresour Technol* 98: 2243–2257
- Allen S, McKay G, Khader K (1989) Intraparticle diffusion of a basic dye during adsorption onto sphagnum peat. *Environ Pollut* 56:39–50
- Amimi M, Younesi H, Bahramifar N (2009) Statistical modeling and optimization of the cadmium biosorption process in an aqueous solution using *Aspergillus niger*. *Colloids Surf A Physicochem Eng Asp* 337:67–73
- Daraei H, Mittal A, Noorisepehr M, Mittal J (2015) Separation of chromium from water samples using eggshell powder as a low-cost sorbent: kinetic and thermodynamic studies. *Desalin Water Treat* 53:214–220
- Ding C, Cheng W, Sun Y, Wang X (2015) Novel fungus-Fe₃O₄ nanobiocomposites as high performance adsorbents for the removal of radionuclides. *J Hazard Mater* 295:127–137
- Dodrill B, Cryotronics LS (1999) *Magnetic media measurements with a VSM*. Lake Shore Cryotronics, Westerville, p 575
- Farooq U, Kozinski JA, Khan MA, Athar M (2010) Biosorption of heavy metal ions using wheat based biosorbents—a review of the recent literature. *Bioresour Technol* 101:5043–5053
- Fatahian S, Shahbazi-Gahrouei D, Pouladian M, Yousefi M, Amiri GR, Noori A (2012) Biodistribution and toxicity assessment of radiolabeled and DMSA coated ferrite nanoparticles in mice. *J Radioanal Nucl Chem* 293:915–921
- Fathima A, Aravindhana R, Rao JR, Nair BU (2015) Biomass of *Termitomyces clypeatus* for chromium (III) removal from chrome tanning wastewater. *Clean Techn Environ Policy* 17:541–547
- Fu F, Wang Q (2011) Removal of heavy metal ions from wastewaters: a review. *J Environ Manag* 92:407–418
- Guan X, Chang J, Chen Y, Fan H (2015) A magnetically-separable Fe₃O₄ nanoparticle surface grafted with polyacrylic acid for chromium (III) removal from tannery effluents. *RSC Adv* 5:50126–50136
- Hlihor RM, Figueiredo H, Tavares T, Gavrilescu M (2017) Biosorption potential of dead and living *Arthrobacter viscosus* biomass in the removal of Cr (VI): batch and column studies. *Process Saf Environ Prot* 108:44–56
- Iconaru SL, Guégan R, Popa CL, Motelica-Heino M, Ciobanu CS, Predoi D (2016) Magnetite (Fe₃O₄) nanoparticles as adsorbents for As and Cu removal. *Appl Clay Sci* 134:128–135
- Kapoor A, Viraraghavan T, Cullimore DR (1999) Removal of heavy metals using the fungus *Aspergillus niger*. *Bioresour Technol* 70: 95–104
- Kurt BZ, Uckaya F, Durmus Z (2017) Chitosan and carboxymethyl cellulose based magnetic nanocomposites for application of peroxidase purification. *Int J Biol Macromol* 96:149–160
- Lefèvre CT, Bazylinski DA (2013) Ecology, diversity, and evolution of magnetotactic bacteria. *Microbiol Mol Biol Rev* 77:497–526
- Li J, Cai F, Lv H, Sun J (2013) Selective competitive biosorption of Au (III) and Cu (II) in binary systems by *Magnetospirillum gryphiswaldense*. *Sep Sci Technol* 48:960–967
- Li Q, Kartikowati CW, Horie S, Ogi T, Iwaki T, Okuyama K (2017) Correlation between particle size/domain structure and magnetic properties of highly crystalline Fe₃O₄ nanoparticles. *Sci Rep* 7: 9894–9900
- Lv Z, Liang C, Cui J, Zhang Y, Xu S (2015) A facile route for the synthesis of mesoporous melamine-formaldehyde resins for hexavalent chromium removal. *RSC Adv* 5:18213–18217
- Mondal NK, Samanta A, Dutta S, Chattoraj S (2017) Optimization of Cr (VI) biosorption onto *Aspergillus niger* using 3-level Box-Behnken design: equilibrium, kinetic, thermodynamic and regeneration studies. *J Genet Eng Biotechnol* 15:151–160
- Nourbakhsh M, Sag Y, Özer D, Aksu Z, Kutsal T, Caglar A (1994) A comparative study of various biosorbents for removal of chromium (VI) ions from industrial waste waters. *Process Biochem* 29:1–5

- Owlad M, Aroua MK, Daud WAW, Baroutian S (2009) Removal of hexavalent chromium-contaminated water and wastewater: a review. *Water Air Soil Pollut* 200:59–77
- Paul S, Bera D, Chattopadhyay P, Ray L (2006) Biosorption of Pb (II) by *Bacillus cereus* M¹¹⁶ immobilized in calcium alginate gel. *J Hazard Subst Res* 5:1–13
- Petcharoen K, Sirivat A (2012) Synthesis and characterization of magnetite nanoparticles via the chemical co-precipitation method. *Mater Sci Eng B* 177:421–427
- Prasenjit B, Sumathi S (2005) Uptake of chromium by *Aspergillus foetidus*. *J Mater Cycles Waste* 7:88–92
- Preethi J, Prabhu SM, Meenakshi S (2017) Effective adsorption of hexavalent chromium using biopolymer assisted oxyhydroxide materials from aqueous solution. *React Funct Polym* 117:16–24
- Rajput S, Pittman CU, Mohan D (2016) Magnetic magnetite (Fe₃O₄) nanoparticle synthesis and applications for lead (Pb²⁺) and chromium (Cr⁶⁺) removal from water. *J Colloid Interface Sci* 468:334–346
- Ramos RL, Jacome LB, Barron JM, Rubio LF, Coronado RG (2002) Adsorption of zinc (II) from an aqueous solution onto activated carbon. *J Hazard Mater* 90:27–38
- Rezaei H (2016) Biosorption of chromium by using *Spirulina sp.* *Arab J Chem* 9:846–853
- Rosales-Landeros C, Barrera-Díaz CE, Bilyeu B, Guerrero VV, Núñez FU (2013) A review on Cr (VI) adsorption using inorganic materials. *Am J Anal Chem* 4:8–16
- Salam MA (2017) Preparation and characterization of chitin/magnetite/multiwalled carbon nanotubes magnetic nanocomposite for toxic hexavalent chromium removal from solution. *J Mol Liq* 233:197–202
- Sivakumar D (2016) Biosorption of hexavalent chromium in a tannery industry wastewater using fungi species. *Global J Environ Sci Manage* 2:105–124
- Sureshkumar V, Daniel SK, Ruckmani K, Sivakumar M (2016) Fabrication of chitosan–magnetite nanocomposite strip for chromium removal. *Appl Nanosci* 6:277–285
- Tan Y, Wei C, Gong Y, Du L (2017) Adsorption of hexavalent chromium onto sisal pulp/polypyrrole composites. *IOP Conference Series: Materials Science and Engineering*. IOP Publishing, pp 012007–0120013
- Wang Y, Gao H, Sun J, Li J, Su Y, Ji Y, Gong C (2011) Selective reinforced competitive biosorption of Ag (I) and Cu (II) on *Magnetospirillum gryphiswaldense*. *Desalination* 270:258–263
- Weber W, Morris J (1962): *Advances in water pollution research*, Proceedings of the First International Conference on Water Pollution Research. Pergamon Press Oxford, pp 231
- Zafar S, Aqil F, Ahmad I (2007) Metal tolerance and biosorption potential of filamentous fungi isolated from metal contaminated agricultural soil. *Bioresour Technol* 98:2557–2561
- Zhang L, He R, Gu H-C (2006) Oleic acid coating on the monodisperse magnetite nanoparticles. *Appl Surf Sci* 253:2611–2617